Structure of a *C. perfringens* Enterotoxin Mutant in Complex with a Modified Claudin-2 Extracellular Loop 2

Tamas S. Yelland [1], Claire E. Naylor [1], Tannya Bagoban [1], Christos G. Savva [1,+], David S. Moss [1], Bruce A. McClane [2], Ingolf E. Blasig [3], M. Popoff [4] and Ajit K. Basak [1]

*1 - **Department of Biological Sciences,** Birkbeck College, London WC1E 7HX, UK*
*2 - **Department of Microbiology and Molecular Genetics,** University of Pittsburgh, Pittsburgh, PA 15261, USA*
*3 - **Leibniz-Institut für Molekulare Pharmakologie im Forshungsverbund Berlin e.V. (FMP),** 13125 Berlin, Germany*
*4 - **Anaerobic Bacteria and Toxins Unit,** Department of Microbiology, Institut Pasteur, 75724 Paris Cedex 15, France*

***Correspondence to Ajit K. Basak:** Department of Biological Sciences, Birkbeck College, Malet Street, London WC1E 7HX, UK. a.basak@mail.cryst.bbk.ac.uk*
http://dx.doi.org/10.1016/j.jmb.2014.07.001
Edited by: T. J. Smith

Abstract

CPE (*Clostridium perfringens* enterotoxin) is the major virulence determinant for *C. perfringens* type-A food poisoning, the second most common bacterial food-borne illness in the UK and USA. After binding to its receptors, which include particular human claudins, the toxin forms pores in the cell membrane. The mature pore apparently contains a hexamer of CPE, claudin and, possibly, occludin. The combination of high binding specificity with cytotoxicity has resulted in CPE being investigated, with some success, as a targeted cytotoxic agent for oncotherapy. In this paper, we present the X-ray crystallographic structure of CPE in complex with a peptide derived from extracellular loop 2 of a modified, CPE-binding Claudin-2, together with high-resolution native and pore-formation mutant structures. Our structure provides the first atomic-resolution data on any part of a claudin molecule and reveals that claudin's CPE-binding fingerprint (NPLVP) is in a tight turn conformation and binds, as expected, in CPE's C-terminal claudin-binding groove. The leucine and valine residues insert into the binding groove while the first residue, asparagine, tethers the peptide via an interaction with CPE's aspartate 225 and the two prolines are required to maintain the tight turn conformation. Understanding the structural basis of the contribution these residues make to binding will aid in engineering CPE to target tumor cells.

Introduction

Clostridium perfringens is a Gram-positive anaerobic spore-forming bacterium that is ubiquitous in nature. It can secrete an array of toxins that vary from strain to strain. This toxin diversity allows *C. perfringens* to cause a range of diseases including human food poisoning, gas gangrene, human enteritis necroticans and enterotoxaemia in livestock.

CPE (*C. perfringens* enterotoxin) is the major virulence determinant for *C. perfringens* type-A food poisoning [1]. This type of food poisoning is a significant problem across the globe, ranking as the second most common bacterial food-borne illness in both the USA and the UK. The Centers for Disease Control and Prevention in the USA estimates that nearly 1 million cases of *C. perfringens* type-A food poisoning occur annually in the USA (Centers for Disease Control and Prevention, *Estimates of Foodborne Illness in the United States*. 2011. 11 June, 2012[†]). It results from consumption of food contaminated with *C. perfringens* strains that produce CPE in the intestines. Two observations confirm that CPE is the responsible toxin. Firstly, inactivation of the *cpe* gene eliminated the enteric pathogenicity of a food poisoning strain in animal models and this attenuation was reversible by complementation [2]. Secondly, ingestion of purified CPE by human volunteers resulted in the gastroenteritis symptoms of type-A food poisoning [3].

CPE is also associated with cases of hospital- and community-acquired AAD (*a*ntibiotic-*a*ssociated

*d*iarrhea) and SD (*s*poradic *d*iarrhea), which are more severe than typical cases of type-A food-borne illness [4]. While the media focuses on AAD and SD caused by strains of *Clostridium difficile*, CPE is also responsible for a significant fraction of hospital-acquired enteric illnesses [5,6]. CPE has also been linked with some veterinary gastrointestinal diseases [7] and, controversially, sudden infant death syndrome [8].

CPE differs from other *C. perfringens* toxins in that it is not a secreted toxin but rather is released at the completion of sporulation upon lysis of the mother cell at which time CPE can represent up to 15% of dry cell mass [9]. This membrane-interacting toxin is a 319-residue polypeptide chain of approximately 35 kDa molecular mass [10]. It can bind to several mammalian cell types via human Claudin-3 or Claudin-4 [11], which belong to the large claudin family of 20- to 27-kDa tight junction proteins [12–14]. Other human claudins have also been shown to bind CPE, though with lower affinity [15]. The high specificity of this interaction has resulted in CPE being identified as a potential biotechnology agent and, in particular, as an oncotherapeutic [16–19]. Understanding the basis for this specificity will result in the potential to alter which claudins recognize CPE and therefore target different cell types, as described in Takahashi *et al*. [20].

Cytotoxicity and cell death, which occur within 30 min of CPE exposure at 37 °C [21], result from alterations in membrane permeability caused by pore formation [11]. In mammalian cells, CPE forms two large complexes named CH-1 and CH-2 [22,23]. Both these two CPE complexes are SDS resistant and their stoichiometry and mass have been the subject of continued study, with recent estimates indicating sizes of approximately 425–500 kDa and 550–660 kDa, for CH-1 and CH-2, respectively. These complexes apparently consist of a CPE hexamer, claudin and, for CH-2, another tight junction protein named occludin [24].

Winkler *et al*. reported that specificity for Claudin-3 and Claudin-4 is provided via a fingerprint sequence (149NPLVP153) in extracellular loop 2 (ECL2) of the claudin [25], while the exact sequence only occurs in mouse Claudin-3 and the amino acids in positions 3, 4 and 5 of the fingerprint can be conservatively substituted. Introduction of this fingerprint by mutation of two residues was sufficient to turn a peptide derived from non-CPE-binding mouse Claudin-2 into a peptide that bound CPE better than the wild-type CPE-binding mouse Claudin-4. Mutation of the fingerprint residues reduces binding of claudin to CPE (Table 1). The involvement of residues outside the fingerprint is not ruled out and other claudins lacking a complete fingerprint are reported to bind CPE, including human Claudin-8 and Claudin-14 [15]. However, these peptides bind to the toxin with reduced affinity, and their affinity for CPE is increased by introducing the canonical fingerprint residues. CPE has been shown to interact with claudin via its C-terminal domain (residues 194–319

Table 1. CPE and Claudin-4 mutations affecting the interaction between them.

Mutation	Methods used	Approximate cytotoxicity as % wild-type activity	Comment	Reference
(a) CPE mutations affecting activity				
Wild type		100		—
Full-length CPE				
Asp48Ala/Asn/Glu	^{86}Rb release	<1		30
Ile51Ala	^{86}Rb release	<1		30
Tyr306Ala	LDH release competition/TEER	64/64		28
Tyr310Ala	LDH release competition/TEER	72/94		28
Tyr312Ala	LDH release competition/TEER	73/100		28
Leu315Ala	LDH release competition/TEER	70/45		28
C-terminal domain only		**Claudin-4 binding as % wild type**		
Leu223Ala	Pull-down	100	Claudin-3 binding 20%	34
Arg227Ala	Pull-down	80	Claudin-3 binding 10%	34
Leu254Ala	Pull-down	80	Claudin-3 binding 30%	34
Asp284Ala	Pull-down	10	Claudin-3 binding 100%	34
(b) Claudin ECL2 mutations affecting C-CPE binding: Numbering as for Claudin-2 ECL2				
Wild type		100		—
Claudin-3				
Asn149Asp	Pull-down	5	Mouse ECL2 peptide	25
Leu151Ala	Pull-down	5	Mouse ECL2 peptide	25
Asn149Asp/Arg158Tyr	^{125}I-CPE binding/TTC cytotoxicity	1	Human full length	39
Asn149Asp	Pull-down	50%	Mouse full length	34
Claudin-4				
Asn149Asp	Cytotoxicity	<1	Human full length	40

[26]). In particular, tyrosines 306, 310 and 312 and leucine 315 in CPE are important for claudin binding [27,28] (Table 1). The structure of the C-terminal domain in isolation has been determined to 1.75 Å [29] and the residues associated with claudin binding reside at the base of a cleft in the C-terminal protein surface. However, the C-terminal domain in isolation is insufficient for cytotoxicity. In the absence of the C-terminal domain (residues 200–319), CPE is not cytotoxic and cannot form active pores [26,29]. In addition, alanine-scanning mutagenesis identified aspartate 48 (D48A) as a key residue for large complex formation [30], while the deletion of up to the first 44 residues from native CPE results in a slight increase in cytotoxicity [31].

Previously, we (and others [32,33]) have determined the structure of full-length CPE (Fig. 1). In all the crystal structures solved to date [32,33], and those in this paper, the CPE forms an intimate trimer, whose interface has the characteristics of a biological significant interface, though this trimer has not yet been shown to have any functional significance. These structures show that residues implicated in claudin binding (Table 1), including Tyr306, Tyr310 and Tyr312, form a pocket on the protein surface. All of these claudin-binding pockets are accessible and on the same side of the trimer. More recent studies on the C-terminal domain have identified a number of residues on the opposite edge of this pocket as also important for binding, including Ser256, Ile258 and Val259 [34] (Table 1).

The full-length structure showed that CPE is a member of the aerolysin-like β pore-forming toxin (βPFT) family. βPFTs are a group of cytotoxic proteins with divergent structures and sequences that are characterized by their common ability to permeabilize cell membranes and ultimately to cause cell death [35]. They all have structurally related oligomerisation domains but unrelated receptor-binding domains. Despite their diverse sequences, these toxins have a common mode of action in that they each possess an amphipathic stretch of residues that, on binding to the appropriate cell surface receptors, forms a β-hairpin that contributes to the membrane-spanning oligomeric β-barrel of the pore. CPE differs slightly from the rest of the group in that the amphipathic residues (residues 81–106) that have been identified as the β-hairpin pore-forming residues [23,36] adopt

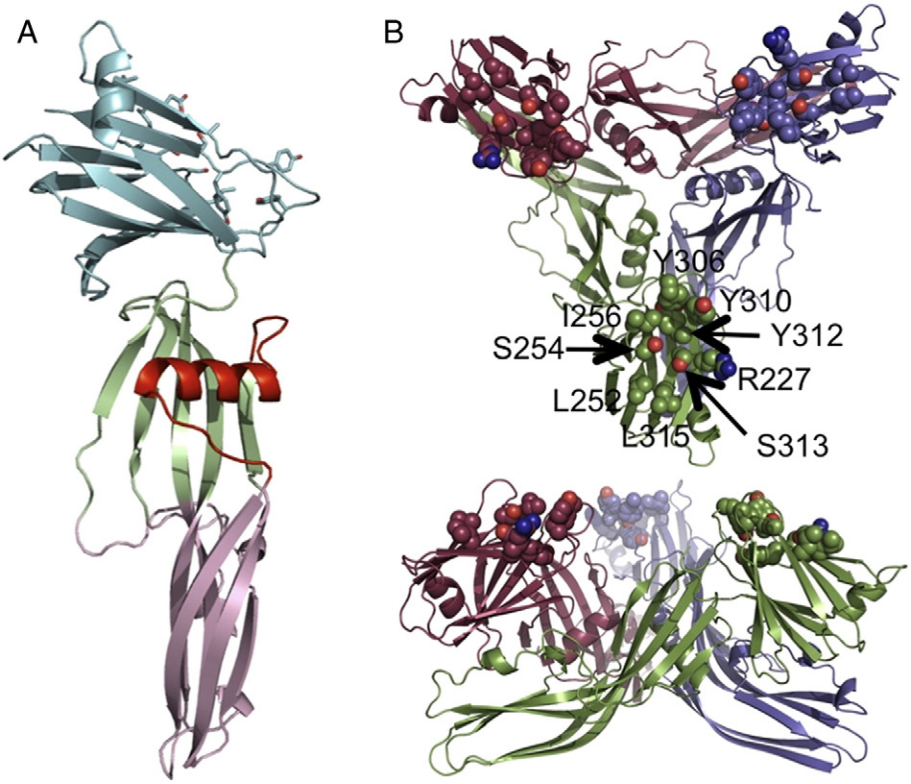

Fig. 1. Structure of full-length CPE. Cartoon representation of (A) the monomer, colored pale green and pink for the oligomerisation domain and light cyan for the C-terminal claudin-binding domain. The membrane-inserting residues are highlighted in red. (B) The trimer seen in the crystal. The monomers are colored green, maroon and violet; the claudin-binding pockets are highlighted by drawing of likely claudin-binding residues as spheres.

a helical conformation in the soluble form, while these residues more normally fold into a β-hairpin in other members of the group.

At high concentrations, CPE is able to form cation-preferring pores in pure lipid bilayers in the absence of receptor claudin or other proteins [37]. Electric current measurements across lipid bilayers containing CPE pores show that it preferentially transports small positive ions, with ions larger than approximately 6.0 Å unable to pass through the CPE pore [37].

In this paper, we present a number of structures. Firstly, that of CPE with the N-terminal 37 residues deleted (ΔN37CPE). This construct is stable and easier to crystallize than full-length CPE, the N-terminal 37 residues are disordered in all the full-length structures solved to date and removal of up to the first 44 amino acids of CPE causes a 2- to 3-fold increase in toxicity [31]. We then look at the structure of the ΔN37CPE with the mutation Asp48Ala introduced and show that the inactivity of this mutant is not due to any major conformational change. Finally, we present the structure of CPE with bound peptide derived from the ECL2 of mouse Claudin-2 (CPE-CLD2), containing two mutations required for CPE binding. The CPE-CLD2 structure shows that the fingerprint sequence is required to form an unusual tight turn conformation in order to allow optimal interaction with the CPE-binding pocket and, for the first time, provides atomic-resolution information on the interaction between CPE and claudin.

Results

ΔN37CPE

ΔN37CPE has increased activity compared to full-length CPE and is more stable and easier to purify, concentrate and crystallize; thus, it has been used for all the studies described here. In order to distinguish changes induced by the loss of 37 N-terminal residues, we first determined the structure of the ΔN37CPE in isolation. ΔN37CPE crystals diffracted to a resolution of 1.9 Å and were in space group *C*2 with cell dimensions $a = 191.7$ Å, $b = 128.3$ Å, $c = 137.2$ Å and $\beta = 133.8°$. The structure was solved by molecular replacement using full-length CPE (PDB ID 2XH6) [32] as a model and revealed six copies of the CPE monomer in the asymmetric unit arranged in two trimers with a solvent content of 58% (v/v). After refinement, the final R/R_{free} was 17.6/19.7%. Further statistics are listed in Table 2 and the coordinates are deposited with PDB ID 3ZIX. The overall structure of the ΔN37CPE monomer is unchanged from that of full-length CPE, in which the N-terminal 34 amino acids were disordered and not visible in the electron density map [32]. In the three structures described in this paper, there are in total 27 crystallographically independent copies of the CPE monomer due to high levels of non-crystallographic symmetry (NCS). Table 3 lists the mean and standard deviation for

Table 2. Data collection and refinement statistics (molecular replacement)

	ΔN37CPE	ΔN37CPE-D48A	CPE-CLD2 complex	
Data collection				
Space group	*C*2	*C*2	*C*2	
Cell dimensions				
a, *b*, *c* (Å)	191.7, 128.3, 137.2	190.6, 128.0, 136.4	369.6, 100.3, 265.4	
α, β, γ (°)	90.0, 133.8, 90.0	90.0, 133.8, 90.0	90.0, 119.7, 90.0	
Resolution (Å)	47.0–1.9 (1.94–1.90)[a]	98.4–1.9 (1.94–1.9)	20.0–3.4 (3.5–3.4)	
R_{sym} or R_{merge}	6.5 (122.0)	14.6 (144.5)	20.7 (77.8)	17.4 (64.3)
$I/\sigma I$	17.42 (1.57)	7.42 (1.26)	5.55 (1.05)	7.7 (1.7)
Completeness (%)	98.2 (95.1)	99.2 (94.8)	81.9 (47.4)	53.7 (9.7)
Redundancy	7.66 (7.34)	7.32 (6.9)	3.4 (1.9)	4.0 (2.65)
Refinement				
Resolution (Å)	47–1.9	49.23–1.9	20–3.4	
No. of reflections	185,641	185,455	96,758	
R_{work}/R_{free}	17.6/19.7	17.5/19.6	20.4/24.0	
No. of atoms				
Protein	13,415	13,397	34,326	
Ligand/ion	1947	1870	0	
Water	1762	1685	0	
B-factors				
Protein	44.4	48.0	117.9	
Ligand/ion	59.9	63.0	n/a	
Water	52.8	56.5	n/a	
RMSD				
Bond lengths (Å)	0.010	0.0096	0.010	
Bond angles (º)	1.09	1.09	1.37	

Number of crystals for each structure should be noted in footnote.
[a] Values for the highest-resolution shell are given in parentheses.

Table 3. Mean and standard deviation for the C^{α} RMSD between each copy of the molecule in Structure 1 and Structure 2

	Full-length CPE [3]	ΔN37CPE [6]	ΔN37CPE-D48A [6]	CPE-CLD2 [15]
(a) Monomers (Å)				
CPE-CLD2 [15]	0.81 ± 0.21	0.72 ± 0.1	0.72 ± 0.09	0.26 ± 0.1
ΔN37CPE-D48A [6]	0.68 ± 0.1	0.34 ± 0.11	0.38 ± 0.07	
ΔN37CPE [6]	0.70 ± 0.09	0.36 ± 0.09		
Full-length CPE [3]	0.56 ± 0.13			
	Full-length CPE [1]	ΔN37CPE [2]	ΔN37CPE-D48A [2]	CPE-CLD2 [5]
(b) Trimers (Å)				
CPE-CLD2 [5]	1.04 ± 0.03	1.1 ± 0.05	1.2 ± 0.09	0.35 ± 0.1
ΔN37CPE-D48A [2]	0.99 ± 0.05	0.15 ± 0.02	0.61 (no SD)	
ΔN37CPE [2]	0.99 ± 0.003	0.57 (no SD)		
Full-length CPE [1]	N/A			

The number of NCS-related copies in each structure is indicated in brackets. DN37CPE: CPE with the N-terminal 37 residues deleted. DN37CPE-D48A: DN37CPE with Asp48 mutated to Ala. CPE-CLD2: DN37CPE complexed with a peptide derived from mouse Claudin-2 extracellular loop 2.

the all C^{α} atom RMSD (*r*oot-*m*ean-*s*quare *d*eviation) between each copy of the monomer in the asymmetric unit for one structure and each copy in a second. Table 3 shows that the CPE monomers in ΔN37CPE are essentially unchanged from those in the full-length CPE.

There are two significant areas of difference between ΔN37CPE and full-length CPE. These differences are present in all chains and are illustrated in Fig. 2. Firstly, though the first N-terminal residue corresponding to the CPE sequence in ΔN37CPE is residue 38, removal of the His-tag added to the sequence for purification left four non-native residues (sequence Gly34-Ala-Met-Gly37) remaining in N-terminus to the first native CPE amino acid. These four residues are ordered and visible in the electron density map for the ΔN37CPE structure and adopt a different conformation from the native residues 34–37 in the full-length CPE structure (sequence Asn34-Ser-Asn-Leu37). In ΔN37CPE, the N-terminus extends toward the C-terminal domain, and this would be sterically prohibited in full-length CPE, and in the full-length structure, residues 34–37 extend into the solvent. It is likely that the presence of the disordered N-terminal peptide extending out toward the C-terminal domain results sterically hinders the binding of the C-terminal domain to claudin and that this reasons its removal results in a slightly more active toxin.

The second difference between the two structures is that Pro191 adopts a *cis* conformation in full-length CPE while it is *trans* in ΔN37CPE (Fig. 2B). The change in conformation results in additional movement in the surrounding chain. This section of CPE is solvent exposed and mediates symmetry interactions in each copy of ΔN37CPE. The *cis* conformation of full-length CPE extends further into solvent and, if maintained in the ΔN37CPE crystal form, would result in a steric clash. Given the small activation energy required to change the conformation of proline, it is likely this steric clash is the cause of the difference.

ΔN37CPE trimer

Full-length CPE forms a trimer in all crystal forms reported to date [32,33]. The six copies of ΔN37CPE in the asymmetric unit of this crystal structure are arranged in two similar trimers. The all C^{α} atom RMSD between these two trimers and that in the full-length CPE is 0.99 Å (Supplementary Fig. 1 and Table 3b) in both cases. This is larger than the mean RMSD between monomers (Table 3a) due to a movement of the C-terminal domain of one monomer in the trimer and the N-terminal domain of a second monomer with which it is interacting. The result is a reduction of space between monomers close to the likely location of the 34 disordered residues in full-length CPE. It is probably the loss of these residues that allows the more tightly packed trimer to form, providing further evidence of the steric hindrance to interactions with other molecules caused by the disordered N-terminal peptide.

ΔN37CPE-D48A

Introduction of the mutation Asp48Ala into CPE has previously been shown to prevent prepore formation and thereby eliminate mature pore formation and cytotoxicity [23,30]. Determination of the full-length CPE structure showed that this residue is solvent exposed and distant from both the predicted claudin-binding site in the C-terminus and from the amphipathic residues (81–106) expected to insert into the membrane [32]. We determined the structure of ΔN37CPE-D48A to identify if the mutation induced any structural changes that would explain the loss of cytotoxicity. ΔN37CPE-D48A crystallized under the same conditions as for ΔN37CPE, and the crystals diffracted to 1.9 Å and had the same space group

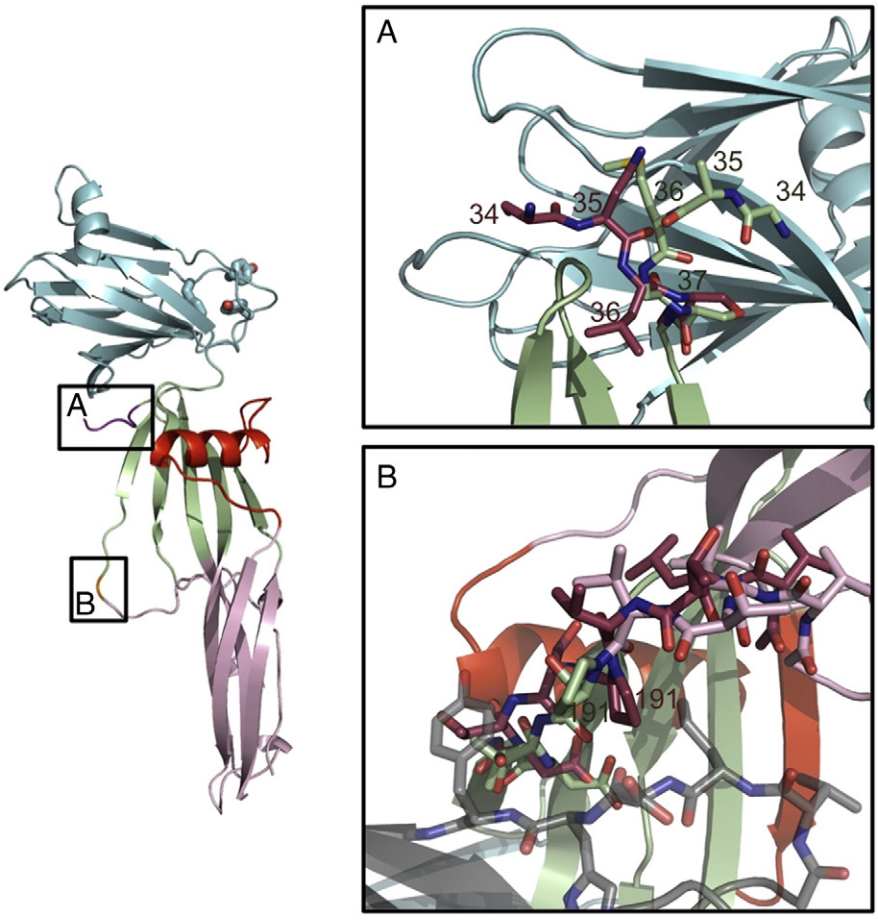

Fig. 2. Differences between the structure of full-length CPE and ΔN37CPE (A) at the N-terminus; the N-terminal domain of full-length CPE is shown in maroon and that for ΔN37CPE is shown in pale green. (B) P191 peptide-flip. The full-length CPE conformation is shown in maroon, and symmetry-related molecules in the ΔN37CPE crystal packing are in semitransparent gray. It is evident that the full-length conformation clashes with these residues. The ΔN37CPE is in pale green, red and cyan and does not clash.

(*C*2) as the ΔN37CPE crystals and very similar cell dimensions of a = 190.6 Å, b = 128.0 Å, c = 136.4 Å and β = 133.8°. Structure solution by molecular replacement revealed a similar arrangement of six CPE monomers in two trimers as for the ΔN37CPE crystals. The R/R_{free} after refinement was 17.5/19.6%, and further statistics are listed in Table 2 and the coordinates are deposited with PDB ID 3ZIW. The mutant ΔN37CPE-D48A monomer and trimer are similar to that of ΔN37CPE as shown by the mean all C^{α} atom RMSD between different copies (Table 3). However, there is clear negative difference electron density indicating the loss of the aspartate side chain at residue 48 (Fig. 3). A recent X-ray structure of another aerolysin-like toxin, *Eisenia fetida* lysenin [38], has identified a sphingomyelin-binding site on one edge of the N-terminal domain. However, when the molecules are compared, this site is on the opposite side of the domain from Asp48. Therefore, no conclusions about the loss of activity in CPE-D48A mutant can be reached from our high-resolution structure. Oligomerisation and membrane insertion will induce conformation in CPE and the Asp48Ala mutation may affect these conformation changes. Alternatively Asp48 may form part of the oligomerisation interface. Further studies are required to identify the role of this residue in CPE cytotoxicity.

Peptide-bound structure (CPE-CLD2 ECL2 variant)

Co-crystallization of ΔN37CPE with a peptide derived from a variant mouse Claudin-2 ECL2 with two-residue changes to increase CPE-binding affinity [25] resulted in a new crystal form.

Many authors have shown that the composition of ECL2 is important for CPE binding, using both chimeric claudins (with ECL2 from one claudin exchanged for that from another) [39] and site-directed mutations [34,40] in full-length claudin. Winkler *et al.* showed that using peptides corresponding to the

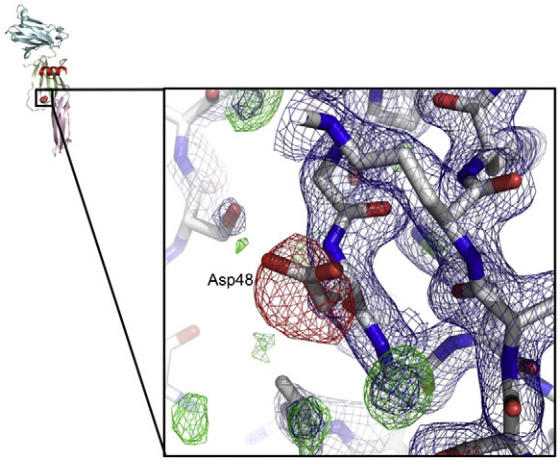

Fig. 3. Difference density for D48A, contoured at +3.0 (green) and −3.0 (red) rms and phases calculated following initial rigid-body refinement. Final $2F_o - F_c$ map for D48A mutant, contoured at 1.5 rms in blue. Asp48 side-chain conformation in Δ37CPE shown as sticks with thin dark-gray bonds.

ECL2 sequence in surface plasmon resonance experiments gave results that reflected binding and cytotoxicity assays using full-length claudin expressed in mammalian cells [25]. Wild-type mouse Claudin-2 (UniProt ID O88552) does not bind CPE [25]. However, mutating Asp149 to Asn and Ser155 to Ala resulted in an ECL2 peptide that bound C-CPE more tightly than the ECL2 peptide derived from a Claudin known to bind CPE. The importance of residue 149 being Asn for CPE-binding mutation has been shown by many researchers [25,34,39,40] (Table 1). The mutations result in a CPE-binding fingerprint identical with that in CPE-binding claudins, and thus, the results seen here are expected to be applicable to CPE–claudin interactions in full-length native CPE. ΔN37CPE was incubated overnight with this peptide (^{141}HGILRDFYNPLVPDAMKFEI^{160}).

Following incubation, crystallization trials resulted in crystals diffracting to 3.4 Å. Data analysis revealed a space group of *C*2 once again but, this time, with cell dimensions of a = 369.6 Å, b = 100.3 Å, c = 265.4 Å and β = 119.7°. Structure solution revealed 15 molecules in the asymmetric unit arranged in five trimers, with a solvent content of 70%. The presence of both high NCS and high solvent content resulted in more detailed maps than what is normally expected at this resolution. Refinement gave an R/R_{free} of 20.4/24.0%, with further statistics provided in Table 2 and the coordinates deposited with PDB ID 4P5H. All the monomers and trimers in the asymmetric unit are essentially identical with each other and similar to the monomer and trimers seen in the higher-resolution ΔN37CPE structure to which they were restrained during refinement (Table 3a and b).

Conformation of CLD2 in the CPE-CLD2 crystals

Difference electron density maps calculated using phases from the initial molecular replacement showed clear difference electron density (more than three times the root-mean-square electron density) at the cleft in the C-terminal domain that has been previously associated with claudin binding [29] (Fig. 4A). The presence of two prolines in the CPE-binding fingerprint of claudin allowed easy identification of these residues in the binding pocket. In addition, the residues in claudin that are most important for CPE binding have been identified in a number of studies [25,34,40]. Several of these studies that went on to mutate CPE residues they hypothesized interacted with the mutated claudin residues and showed this restored function. These studies allowed us to assign side chains to claudin residues based on the CPE residues they interacted with. Figure 4C shows the final $2F_o - F_c$ map, while the interactions between the protein and peptide are illustrated in Fig. 4B and D. Strong density is present in each of the 15 binding grooves for the residues of the mutant CLD2-derived peptide that have been shown to be essential for CPE binding [25], in particular, the fingerprint residues 149–153 (NPLVP), which can only tolerate conservative mutations, as discussed below. As the CLD2-derived peptide extends away from CPE and into solvent, the NCS relationship between the copies breaks down, and in most cases, it has not been possible to reconstruct its entire length. Residues leading away from the fingerprint toward N- and C-termini can clearly be seen to be adopting a helical conformation, but NCS between CLD2 copies breaks down as distance from the groove increases, resulting in a loss of electron density map quality so that we have been unable to build these helical parts of the peptide into the electron density map. We will therefore concentrate our discussion on the fingerprint residues (149–153) and well-ordered mutant CLD2-derived peptide residues either side that interact with CPE. In the remainder of Results and Discussion, residues from the CLD2-derived peptide will be prefaced with cld, while those from CPE will be prefaced cpe for clarity.

The formation of the CPE-CLD2 complex buries on average, 390 Å^2 of CPE's solvent-accessible surface in each monomer. The peptide is tethered at either end by possible electrostatic interactions, in particular, between cldAsn149 and cpeAsp225 and cldAsp154 and cpeTyr310. However, the interaction is overwhelming hydrophobic in nature (Fig. 4D), with cldVal152 and cldPro153 packing into first identified binding pocket [29]. cldVal152 packs against cpeIle258, cpeVal259 and cpeTyr312 while cldPro153 stacks against cpeTyr306 and cpeTyr310.

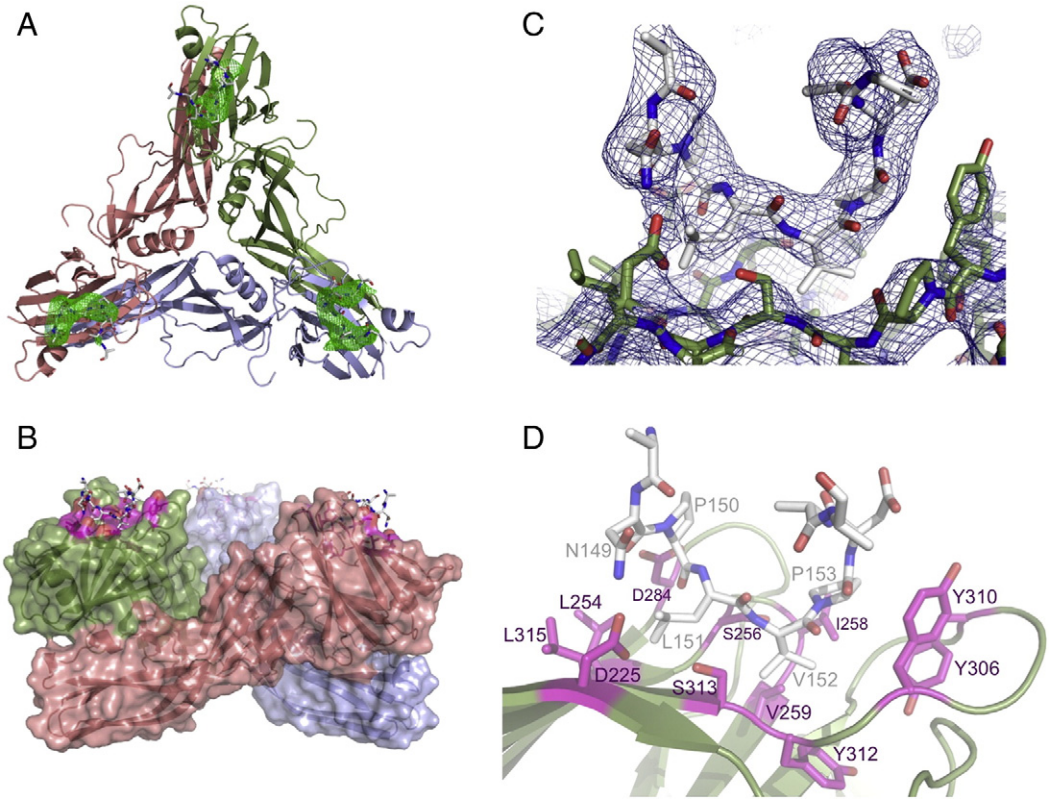

Fig. 4. (A) Difference map showing typical density (contoured in green at 3.0 rms) for claudin-derived peptide for a typical one of the five trimers in the peptide-bound asymmetric unit. Trimer is shown as cartoon representation. (B) One of the five trimers in the asymmetric unit showing CPE as cartoon representation with semitransparent surface representation and the final claudin-derived peptide in stick representations, with peptide-interacting residues in magenta. (C) Final refined $2F_o - F_c$ electron density map contoured at 1.5 rms in dark blue with final refined coordinates shown as sticks, protein with green bonds and claudin-derived peptide with white colored bonds. (D) Stick representation of final refined peptide-bound structure, colored as in (B) with cpe residues that interact with claudin colored magenta and labeled.

cldLeu151 is inserted into the pocket recently identified by Veshnyakova *et al.* [34], including residues cpeLeu254 and cpeLeu315, confirming their analysis of the importance of these residues.

There is a constriction in the claudin-binding groove of CPE, as a result of the side chain of cpeSer313 protruding into it, which separates the originally identified pocket formed by residues including cpeTyr306, cpeTyr310 and cpeTyr312 from the newly identified and slightly shallower pocket containing cpeLeu254 and cpeLeu315. This constriction defines the orientation of cldVal152 needed for insertion into CPE's claudin-binding groove. The required orientation is achieved by presentation of these two residues (cldLeu151 and cldVal152) at the apex of a tight turn. Of the five residues in the claudin NPLVP fingerprint associated with CPE binding (cld residues 149–153), both cldPro150 and cldPro153 are required to form the tight turn that allows cldLeu151 and cldVal152 to insert into the correct pockets in CPE's claudin-binding groove, with cldPro150 adopting a *cis* conformation.

Discussion

Effect of N-terminal residues on CPE cytotoxicity

It has been shown that the deletion of the N-terminal 37 residues from CPE results in 2- to 3-fold increased cytotoxicity [31]. Previously determined structures of CPE have shown that the N-terminal 37 residues of CPE are disordered [32,33]. The structure of ΔN37CPE presented here reveals that the absence of these residues has no significant effect on the rest of the CPE structure. However, the presence of the disordered residues in full-length CPE can be inferred from the changes in orientation between the N- and C-terminal domains and the change in conformation of the ordered N-terminal residues between the full-length and ΔN37CPE structures. The presence of this 37-residue disordered peptide inhibits CPE oligomerization, as what has been shown by Kokai-Kun and McClane [26], probably through steric hindrance of claudin receptor binding.

Implications of the CPE-CLD2 complex structure

While the mutated mouse Claudin-2-derived peptide used in these studies binds more tightly than other peptides, it has been reported that cell lines expressing mouse Claudin-3, Claudin-4, Claudin-7 or Claudin-8 or human Claudin-4 are all highly sensitive to CPE exposure [39] and peptides derived from ECL2 of mouse Claudin-3, Claudin-6, Claudin-7, Claudin-9 and Claudin-14 bind to CPE [25] with various levels of affinity. Claudin peptides with a five-residue fingerprint of the form NP[L/M][V/T/L][P/A] show the highest affinity for CPE. Asparagine at position 1 of the fingerprint is required to form the necessary stabilizing interaction with cpeAsp225, and proline at position 2 is required as this residue contains a *cis* peptide. The next two residues are required to be medium-sized hydrophobic residues to fit into the pockets on the CPE C-terminal domain surface, and finally, the residue at position 5 in the fingerprint is required to form a tight turn but does not adopt a *cis* conformation so that either a proline or an alanine residue can be substituted at this point.

Additional residues in claudin are also involved in the interaction, for example, Claudin-8 can still bind CPE, all be it with reduced affinity, despite lacking a complete CPE-binding fingerprint [15]. In Claudin-8, the fingerprint residues have the sequence NSIVN and it should be noted that replacement of the serine for the correct fingerprint residue, proline, significantly increases the affinity of Claudin-8 for CPE. The same study [15] showed that Claudin-14 also binds CPE, at reduced affinity, compared to Claudin-3 and Claudin-4, despite having a complete CPE-binding fingerprint. It highlighted the mutation of cldAsp146, N-terminal to the fingerprint to Asn in Claudin-14, and showed that restitution of the more common Asp at this position restored CPE-binding affinity. cldAsp146 is not visible in these electron density maps so that we are not able to comment on the likely reason for this.

Takahashi *et al*. introduced mutations into a fragment of CPE (residues 116–319) called C-CPE, to create a broad-spectrum claudin-binding protein [20]. One of the mutations was cpeSer313His. The larger residue will likely completely obscure the cpeTyr306/310/312 binding pocket, which we have shown to confer specificity on CPE. The loss of this pocket therefore effectively removes binding specificity. The remaining mutations were at CPE residues 304, 305, 307 and 309 and introduced a number of positively charged residues. These residues are outside of the specificity-conferring pocket and have likely formed an entirely new, predominantly electrostatic, recognition site for claudins in general.

The binding of a claudin peptide to CPE was modeled and the predicted binding orientation was tested by introducing mutations into both CPE and the claudin loop in a study published by Veshnyakova *et al*. [34]. Our CPE-CLD2 complex structure shows the peptide bound in the pocket in the opposite orientation to which their modeling suggested (with the pockets containing cldLeu151 and cldVal152 swapped). However, the orientation of the cldLeu152 in the smaller pocket as observed by X-ray crystallography leaves sufficient room to accommodate the Leu152Phe mutation that their model suggested it could not. In addition, Veshnyakova *et al*. showed that the mutation cldAsn149Asp reduced binding to the C-terminal domain of CPE [34]. Their model proposed that cldAsn149 and cpeAsp284 would be interacting, but complementary mutations of these two residues failed to rescue Claudin binding. In contrast, in our structure, cpeAsp284 is positioned so that it is only able to interact with Claudin peptide main chain so that it could not rescue cldAsn149Asp binding, while cpeAsp225 is interacting with cldAsn149, explaining why mutation to Asp is deleterious.

Kimura *et al*. noted that the claudin-binding groove of CPE has a negative electrostatic charge [39]. They altered the electrostatic charge in ECL2 and showed that increasing the electronegativity in this loop decreased binding. However, we show that one of the mutations they made (Asn149Asp), which has been shown by many others to eliminate CPE binding in normally CPE sensitive claudins, has a direct interaction with CPE. The other mutation, Arg158Tyr, is further from the peptide-binding groove in our structure and is not ordered. However, we note that others have shown that introduction of a charged residue at this point does not alter C-CPE binding in the absence of the Asn149Asp mutation [25] and that the Claudin-2 ECL2-derived peptide we have used in these studies has the hydrophobic, Phe, in this position. Therefore, it seems likely that work provides further evidence that Asn149 is essential for CPE binding rather than electrostatics being of primary importance in the CPE–claudin interaction.

Implications for pore insertion

(i) Bound polyethylene glycol molecules: -We have identified a number of bound polyethylene glycol (PEG) molecules in both the ΔN37CPE and the ΔN37CPE-D48A structures. There are six well-ordered PEG molecules in each structure at each of the interfaces between molecules in both trimers (Fig. 5). These molecules have direct interactions with the amphipathic sequence that has been shown to be involved in membrane insertion (residues 81–106). In addition, there are less well-ordered PEG molecules bound to the C-terminal domain on the same face as residues known to be important for claudin binding. PEG is an amphipathic molecule and may be mimicking the recognition of

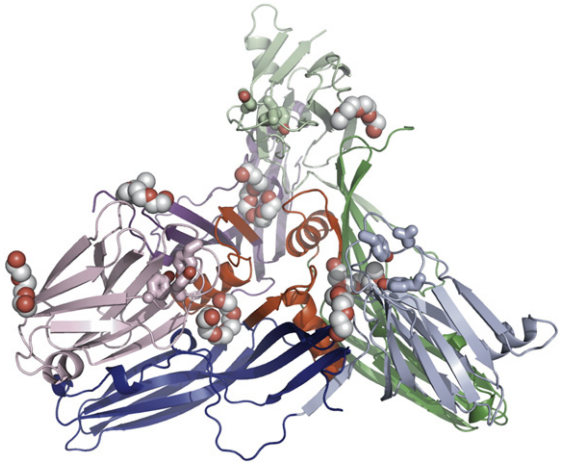

Fig. 5. Cartoon representation of one of the trimer from the ΔN37CPE crystal form. N-terminal domain in lighter shades, C-terminal domain in darker shades. Bound PEG molecules are shown in atom-colored spheres (carbon gray). The location of the PEG molecules is similar in both trimers in the Δ37CPE asymmetric unit and in both trimers in the D48A asymmetric unit. The claudin-binding pockets of the CPE molecules are indicated by bond representation of cpeTyr306, cpeTyr310 and cpeTyr312, colored the same as each C-terminal domain.

phospholipid headgroups following the initial binding of CPE to cell membrane surfaces.

(ii) CPE packing arrangement in the crystal: - The packing of the CPE-CLD2 complex in the asymmetric unit is very interesting as it hints at a role for cpeAsp48. The five trimers in each asymmetric unit are packed in a helix with a 72° turn between each successive trimer, resulting in the five-trimer repeat (Supplementary Fig. 2).

The ΔN37CPE-D48A mutant structure described above showed that the mutation cpeAsp48Ala does not affect the protein fold. The ΔN37CPE-D48A structure and previous CPE structures [32,33] have shown that cpeAsp48 is solvent exposed and distant from the claudin-binding pockets in the same monomer and trimer, from the recently identified lipid binding site on another aerolysin-like βPFT, lysenin [38], and from the likely membrane-inserting residues 81–106. However, cpeAsp48 in one trimer is just 6 Å from the claudin-derived peptide bound to the adjacent trimer in the helix (Fig. 6A and B). While in the peptide-bound structure, the membrane-inserting residues 81–106 are buried, and therefore, a conformation change will be necessary to form the prepore, and the importance of cpeAsp48 for both cytotoxicity and maintaining the helical interactions seen in the crystal suggests that the helix may represent an initial claudin-bound form of CPE. In tight junctions within a cell–cell contact, claudin has been shown to form a “strand and groove” architecture. However, the protein assembly within the tight junctions is so tightly packed by the *trans* interactions between the extracellular loops of the claudin molecules that CPE cannot penetrate into this structure [25]. The latter work showed that CPE associates to claudin oligomers at the cell membrane outside the tight junctions. Based on this and the CPE trimer helix described above, a scheme of the proposed interaction is depicted in Fig. 6C.

In Conclusion

The results we present here show for the first time the conformation of a peptide derived from claudin ECL2 bound to CPE. In addition to the valuable information, it provides about the molecular determinants of the highly specific interaction between CPE and Claudin-3 and Claudin-4, our work provides the first experimental atomic-resolution data for any claudin and shows that ECL2 has an unusual conformation that is important for its interaction with CPE. We have presented here three structures of CPE mutants, determined from crystals grown under conditions different from those of the first full-length CPE structures. There are several copies of the CPE monomer in each of the asymmetric units, and in all cases, they are contained in the same intimate trimer seen in the initial structures. While this trimer is certainly not the membrane active form, its persistence in all atomic-resolution structures of CPE suggests that it may have some biological relevance, for example, in pore formation. Finally, the unusual packing of the CPE-CLD2 complex in the crystals reveals an interaction of cpeAsp48 with claudin-derived peptide bound to the claudin-binding pocket of a CPE molecule in a different trimer.

Materials and Methods

Cloning

The full-length CPE gene was polymerase chain reaction (PCR) amplified from *C. perfringens* strain 8-6 and cloned into pGEX2T. Using this template, we generated a truncated CPE construct (residues 37–319). A ΔN37CPE construct was created from this using forward (NcoI) 5′-CATGC CATGGGCAGTGATGGATTATATG-3′ and reverse (XhoI) 5′-CCGCTCGAGTTAAAATTTTTGAAATAATATTG-3′ oligonucleotide primers (synthesized by MWG Eurofins) with which a PCR for 25 cycles was performed. The reaction product was run on an agarose gel and a gel extraction (Qiagen) protocol was followed. The vector pHis [41] and the PCR product were digested with NcoI and XhoI before ligating the two together. Positive clones were sequenced to ensure that no mutations were introduced. The resultant

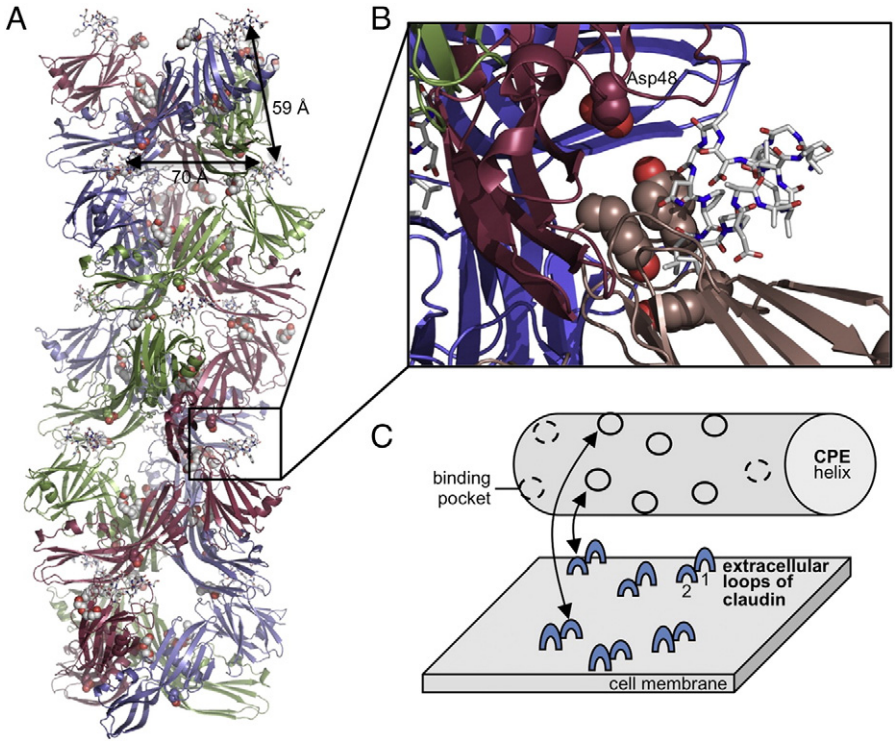

Fig. 6. (A) Cartoon representation of trimer helix in the asymmetric unit, with claudin-derived peptides shown as sticks and Asp48 and Tyr306, Tyr310 and Tyr312 as atom spheres. The location of PEG as seen in the ΔN37CPE structure is shown as yellow sticks. Distances between claudin-binding sites both within the trimer and between adjacent trimers in the helix are indicated. (B) Close up of (a), with monomer to which peptide is bound colored pale pink and monomer from the adjacent trimer colored maroon. (C) Scheme of the potential interaction between CPE trimer helix and claudin oligomers and the membrane surface of a claudin expressing cell outside of cell–cell contacts.

construct had a recombinant tobacco etch virus (rTEV) cleavable His_6-tag on the N-terminus.

D48A mutant

Using the ΔN37CPE construct, we mutated aspartate 48 to alanine using the QuikChange method (Agilent Technologies). Primers 5′-GTAATAGATAAAGGAGCT GGTTGGATATTAGGGGAACC-3′ and 5′-GGTT CCCCTAATATCCAACCAGCTCCTTTATCTATTAC-3′ were utilized to introduce the mutation.

Protein expression and purification

Protein was expressed in *Escherichia coli* BL21 (DE3) cell line. Cells were grown to an OD_{600} of 0.7 ± 0.1 at 37 °C with vigorous shaking, before cooling at room temperature for 30 min. Cells were induced using IPTG to a final concentration of 0.5 mM and grown overnight at 26 ºC shaking at 170 RPM. Cells were pelleted and stored at −20 °C.

Cell pellets were re-suspended on ice in ice-cold lysis buffer [50 mM Tris–HCl (pH 7.5), 500 mM NaCl and protease inhibitor cocktail (Roche Bioscience)]. Re-suspended cells were lysed by passing through a homogenizer twice to ensure complete cell lysis. Cell lysate was sonicated for three 30-s bursts with a 1-min rest period between each burst. The insoluble fraction was removed by centrifugation at 18,000 RPM using a Sorvall RC+ with a F21A-8x50y rotor at 4 °C. The resultant supernatant was filtered through a 0.44-μm filter (Millipore) to remove any remaining insoluble material. The supernatant was loaded onto a HisTrap (GE Healthcare) 5-mL column and eluted with a stepwise gradient of imidazole [4%, 8% and finally a gradient up to 100% of 500 mM in a buffer also containing 20 mM Tris–HCl (pH 7.5) and 500 mM NaCl]. The fractions containing CPE were pooled and dialysed overnight at 4 °C in 20 mM Tris–HCl (pH 7.5), 150 mM NaCl and 2 mM β-mercaptoethanol. ΔN37CPE was also dialysed in the presence of rTEV to remove the His_6-tag in a weight ratio of 25:1 (ΔN37CPE: rTEV). The resultant solution was passed through a HisTrap (GE Healthcare) 5-mL column and the flowthrough was collected. The flowthrough was concentrated using a 10-kDa molecular mass cutoff concentrator (Millipore) and loaded onto a Superdex S200 size-exclusion column. The gel-filtration column was washed with a buffer containing 20 mM Tris–HCl (pH 7.5), 150 mM NaCl and 1 mM DTT. Fractions containing CPE were pooled and concentrated to 20 mg/mL, and their purity was verified by native gel and the protein was then stored at −80 °C.

Crystallization

ΔN37CPE, ΔN37CPE-D48A and CPE-CLD2 were screened for crystallization conditions using Hampton Research Crystal Screen I and II, JCSG and PACT, promising conditions were optimized using the hanging-drop technique with 2 μL of 20 mg/mL protein and 1 μL mother liquor, the well-contained 100 μL mother liquor. Crystals of ΔN37CPE and ΔN37CPE-D48A grew at 16 °C from mother liquor containing 25% (w/v) PEG, with an average molecular mass of 1500 Da (PEG 1500) buffered by 100 mM SPG buffer (succinic acid, sodium dihydrogen phosphate and glycine in the ratio 2:7:7) at pH 6.0. For CPE-CLD2, protein was incubated overnight at 4 °C with 1 mM peptide (sequence: HGILRDFYNPLVPDAMKFEI) supplied by Biosynthesis (Lewisville, TX, USA) before setting up crystallization trials as described above with mother liquor containing 22% (v/v) 2-methyl-2,4-pentanediol and 200 mM ammonium acetate buffered by 100 mM sodium citrate (pH 5.7). Prior to freezing, we cryoprotected crystals by soaking them in mother liquor supplemented by 15% (v/v) PEG 400. The peptide was taken from ECL2 of mouse Claudin-2 141–168, which does not bind CPE; however, two serines were replaced by an asparagine and an alanine (underlined in the sequence mentioned above) recreating the CPE-binding fingerprint from Claudin-3 [25].

Data collection, phasing and refinement

All datasets were collected at the European Synchrotron Radiation Facility (Grenoble, France) on beamlines ID23-2 (ΔN37CPE) and ID29 (ΔN37CPE-D48A and CPE-CLD2) and indexed, integrated and scaled with XDS software suite [42]. Both ΔN37CPE and ΔN37CPE-D48A belonged to the same crystal symmetry and diffracted to 1.9 Å. The space group was *C*2 and the cell dimensions were a = 191.7 Å, b = 128.3 Å, c = 137.2 Å and β = 133.8° for ΔN37CPE and a = 190.6 Å, b = 128.0 Å, c = 136.4 Å and β = 133.8° for ΔN37CPE-D48A. ΔN37CPE was solved by molecular replacement with Phaser [43 using a monomer from our original CPE structure [32] (PDB ID 2XH6) as a model. It revealed that there were six molecules in the asymmetric unit, corresponding to a Matthew's volume of 2.9 $Å^3$/Da and a solvent content of 58% (v/v). The mutant ΔN37CPE-D48A data are isomorphous with the ΔN37CPE data; thus, the refined ΔN37CPE coordinates were subjected to rigid-body refinement against the ΔN37CPE-D48A data with Buster version 1.10.0 [44] resulting in both *R*-factor and R_{free} of 27.6%. Data processing statistics are listed in Table 2.

The CPE-CLD2 complex crystallized in a different form, also space group *C*2, but with cell dimensions a = 369.6 Å, b = 100.3 Å, c = 265.4 Å and β = 119.7°. The data were integrated and scaled with XDS [42] to resolution of 3.4 Å. The CPE-CLD2 complex structure was solved by molecular replacement with Phaser [43] and a trimer of the refined ΔN37CPE coordinates and gave 15 CPE monomers in the asymmetric unit with a Matthew's volume of 4 $Å^3$/Da and a solvent content of 70%. Statistics are listed in Table 2.

Following structure solution, we refined all three models with Buster [44] with NCS restraints [45] and rebuilt them in Coot [46]. In the case of the lower-resolution CPE-CLD2, we also dataset restraints to the higher-resolution native structure, ΔN37CPE, employed [45]. The final R/R_{free} was 17.6/19.7% for ΔN37CPE, was 17.5/19.6% for ΔN37CPE-D48A and was 20.4/24.0% for CPE-CLD2. Further refinement statistics are provided in Table 2.

Accession numbers

The structures described in this paper have been submitted to the Protein Data Bank with the following IDs: ΔN37CPE, 3ZIX; ΔN37CPE-D48A, 3ZIW; and CPE-CLD2, 4P5H.

Supplementary data to this article can be found online at http://dx.doi.org/10.1016/j.jmb.2014.07.001.

Acknowledgements

The authors wish to acknowledge the Medical Research Council for funding C.E.N. (project G0700051), the Wellcome Trust for funding C.G.S. and A.K.B. (project WT089618MA) and National Institutes of Health for supporting B.Mc (grant R37 AI19844-30).

Received 18 March 2014;
Received in revised form 25 June 2014;
Accepted 7 July 2014
Available online 11 July 2014

Keywords:
enterotoxin;
claudin;
receptor;
complex;
structure

✚Present address: C. G. Savva, Laboratory of Molecular Biology, Francis Crick Road, Cambridge CB2 0QH, UK.

†Available from http://www.cdc.gov/foodborneburden/2011-foodborne-estimates.html.

Abbreviations used:
ECL2, extracellular loop 2; βPFT, β pore-forming toxin; NCS, non-crystallographic symmetry; PEG, polyethylene glycol; rTEV, recombinant tobacco etch virus.

References

[1] Adak GK, Long SM, O'Brien SJ. Trends in indigenous foodborne disease and deaths, England and Wales: 1992 to 2000. Gut 2002;51:832–41.

[2] Sarker MR, Carman RJ, McClane BA. Inactivation of the gene (*cpe*) encoding *Clostridium perfringens* enterotoxin eliminates the ability of two *cpe*-positive *C. perfringens* type A human gastrointestinal disease isolates to affect rabbit ileal loops. Mol Microbiol 1999;33:946–58.

[3] Skjelkvale R, Uemura T. Experimental diarrhoea in human volunteers following oral administration of *Clostridium perfringens* enterotoxin. J Appl Bacteriol 1977;43:281–6.
[4] Carman RJ. *Clostridium perfringens* in spontaneous and antibiotic-associated diarrhoea of man and other animals. Rev Med Microbiol 1997;8:S46–8.
[5] Brett MM, Rodhouse JC, Donovan TJ, Tebbutt GM, Hutchinson DN. Detection of *Clostridium perfringens* and its enterotoxin in cases of sporadic diarrhoea. J Clin Pathol 1992;45:609–11.
[6] Mpamugo O, Donovan T, Brett MM. Enterotoxigenic *Clostridium perfringens* as a cause of sporadic cases of diarrhoea. J Med Microbiol 1995;43:442–5.
[7] Songer JG. Clostridial enteric diseases of domestic animals. Clin Microbiol Rev 1996;9:216–34.
[8] Murrell TG, Ingham BG, Moss JR, Taylor WB. A hypothesis concerning *Clostridium perfringens* type A enterotoxin (CPE) and sudden infant death syndrome (SIDS). Med Hypotheses 1987;22:401–13.
[9] McClane B. *Clostridium perfringens*. In: Doyle MP, Beuchat LR, editors. Food Microbiology: Fundamentals and Frontiers. 3rd edit. Washington, DC: ASM Press; 2007. p. 423–44.
[10] Czeczulin JR, Hanna PC, McClane BA. Cloning, nucleotide sequencing, and expression of the *Clostridium perfringens* enterotoxin gene in *Escherichia coli*. Infect Immun 1993;61:3429–39.
[11] McClane BA. The complex interactions between *Clostridium perfringens* enterotoxin and epithelial tight junctions. Toxicon 2001;39:1781–91.
[12] Tsukita S, Furuse M, Itoh M. Multifunctional strands in tight junctions. Nat Rev Mol Cell Biol 2001;2:285–93.
[13] Van Itallie CM, Anderson JM. Claudins and epithelial paracellular transport. Annu Rev Physiol 2006;68:403–29.
[14] Krause G, Winkler L, Mueller SL, Haseloff RF, Piontek J, Blasig IE. Structure and function of claudins. Biochim Biophys Acta 2008;1778:631–45.
[15] Shrestha A, McClane BA. Human claudin-8 and -14 are receptors capable of conveying the cytotoxic effects of *Clostridium perfringens* enterotoxin. MBio 2013(4). http://dx.doi.org/10.1128/mBio.00594-12.
[16] Hashimi SM, Yu S, Alqurashi N, Ipe DS, Wei MQ. Immunotoxin-mediated targeting of claudin-4 inhibits the proliferation of cancer cells. Int J Oncol 2013;42:1911–8.
[17] Lal-Nag M, Battis M, Santin AD, Morin PJ. Claudin-6: a novel receptor for CPE-mediated cytotoxicity in ovarian cancer. Oncogenesis 2012;1:e33.
[18] Neesse A, Hahnenkamp A, Griesmann H, Buchholz M, Hahn SA, Maghnouj A, et al. Claudin-4-targeted optical imaging detects pancreatic cancer and its precursor lesions. Gut 2013;62:1034–43.
[19] Gao Z, McClane BA. Use of *Clostridium perfringens* enterotoxin and the enterotoxin receptor-binding domain (C-CPE) for cancer treatment: opportunities and challenges. J Toxicol 2012;2012:981626.
[20] Takahashi A, Saito Y, Kondoh M, Matsushita K, Krug SM, Suzuki H, et al. Creation and biochemical analysis of a broad-specific claudin binder. Biomaterials 2012;33:3464–74.
[21] McClane BA, Wnek AP. Studies of *Clostridium perfringens* enterotoxin action at different temperatures demonstrate a correlation between complex formation and cytotoxicity. Infect Immun 1990;58:3109–15.
[22] Singh U, Van Itallie CM, Mitic LL, Anderson JM, McClane BA. CaCo-2 cells treated with *Clostridium perfringens* enterotoxin form multiple large complex species, one of which contains the tight junction protein occludin. J Biol Chem 2000;275:18407–17.
[23] Smedley JG, Uzal FA, McClane BA. Identification of a prepore large-complex stage in the mechanism of action of *Clostridium perfringens* enterotoxin. Infect Immun 2007;75:2381–90.
[24] Robertson SL, Smedley JG, Singh U, Chakrabarti G, Van Itallie CM, Anderson JM, et al. Compositional and stoichiometric analysis of *Clostridium perfringens* enterotoxin complexes in Caco-2 cells and claudin 4 fibroblast transfectants. Cell Microbiol 2007;9:2734–55.
[25] Winkler L, Gehring C, Wenzel A, Muller SL, Piehl C, Krause G, et al. Molecular determinants of the interaction between *Clostridium perfringens* enterotoxin fragments and claudin-3. J Biol Chem 2009;284:18863–72.
[26] Kokai-Kun JF, McClane BA. Determination of functional regions of *Clostridium perfringens* enterotoxin through deletion analysis. Clin Infect Dis 1997;25:S165–7.
[27] Harada M, Kondoh M, Ebihara C, Takahashi A, Komiya E, Fujii M, et al. Role of tyrosine residues in modulation of claudin-4 by the C-terminal fragment of *Clostridium perfringens* enterotoxin. Biochem Pharmacol 2007;73:206–14.
[28] Takahashi A, Komiya E, Kakutani H, Yoshida T, Fujii M, Horiguchi Y, et al. Domain mapping of a claudin-4 modulator, the C-terminal region of C-terminal fragment of *Clostridium perfringens* enterotoxin, by site-directed mutagenesis. Biochem Pharmacol 2008;75:1639–48.
[29] Van Itallie CM, Betts L, Smedley JG, McClane BA, Anderson JM. Structure of the claudin-binding domain of *Clostridium perfringens* enterotoxin. J Biol Chem 2008;283:268–74.
[30] Smedley JG, McClane BA. Fine mapping of the N-terminal cytotoxicity region of *Clostridium perfringens* enterotoxin by site-directed mutagenesis. Infect Immun 2004;72:6914–23.
[31] Kokai-Kun JF, McClane BA. Deletion analysis of the *Clostridium perfringens* enterotoxin. Infect Immun 1997;65:1014–22.
[32] Briggs DC, Naylor CE, Smedley JG, Lukoyanova N, Robertson S, Moss DS, et al. Structure of the food-poisoning *Clostridium perfringens* enterotoxin reveals similarity to the aerolysin-like pore-forming toxins. J Mol Biol 2011;413:138–49.
[33] Kitadokoro K, Nishimura K, Kamitani S, Fukui-Miyazaki A, Toshima H, Abe H, et al. Crystal structure of *Clostridium perfringens* enterotoxin displays features of beta-pore-forming toxins. J Biol Chem 2011;286:19549–55.
[34] Veshnyakova A, Piontek J, Protze J, Waziri N, Heise I, Krause G. Mechanism of *Clostridium perfringens* enterotoxin interaction with claudin-3/-4 protein suggests structural modifications of the toxin to target specific claudins. J Biol Chem 2012;287:1698–708.
[35] Anderluh G, Lakey JH. Disparate proteins use similar architectures to damage membranes. Trends Biochem Sci 2008;33:482–90.
[36] Chen J, Theoret JR, Shrestha A, Smedley JG, McClane BA. Cysteine-scanning mutagenesis supports the importance of *Clostridium perfringens* enterotoxin amino acids 80 to 106 for membrane insertion and pore formation. Infect Immun 2012;80:4078–88.
[37] Hardy SP, Ritchie C, Allen MC, Ashley RH, Granum PE. *Clostridium perfringens* type A enterotoxin forms mepacrine-sensitive pores in pure phospholipid bilayers in the absence of putative receptor proteins. Biochim Biophys Acta 2001;1515:38–43.
[38] De Colibus L, Sonnen AF, Morris KJ, Siebert CA, Abrusci P, Plitzko J, et al. Structures of lysenin reveal a shared evolutionary

origin for pore-forming proteins and its mode of sphingomyelin recognition. Structure 2012;20:1498–507.
[39] Kimura J, Abe H, Kamitani S, Toshima H, Fukui A, Miyake M, et al. *Clostridium perfringens* enterotoxin interacts with claudins via electrostatic attraction. J Biol Chem 2010;285:401–8.
[40] Robertson SL, Smedley JG, McClane BA. Identification of a claudin-4 residue important for mediating the host cell binding and action of *Clostridium perfringens* enterotoxin. Infect Immun 2010;78:505–17.
[41] Sheffield P, Garrard S, Derewenda Z. Overcoming expression and purification problems of RhoGDI using a family of "parallel" expression vectors. Protein Expression Purif 1999;15:34–9.
[42] Kabsch W. Xds. Acta Crystallogr Sect D Biol Crystallogr 2010;66:125–32.
[43] McCoy AJ, Grosse-Kunstleve RW, Adams PD, Winn MD, Storoni LC, Read RJ. Phaser crystallographic software. J Appl Crystallogr 2007;40:658–74.
[44] Bricogne G, Blanc E, Brandl M, Flensburg C, Keller PA, Paciorek W, et al. Buster. 1.10.0 edit. Cambridge, UK: Global Phasing Ltd; 2011.
[45] Smart OS, Womack TO, Flensburg C, Keller P, Paciorek W, Sharff A, et al. Exploiting structure similarity in refinement: automated NCS and target-structure restraints in BUSTER. Acta Crystallogr Sect D Biol Crystallogr 2012;68:368–80.
[46] Emsley P, Lohkamp B, Scott WG, Cowtan K. Features and development of Coot. Acta Crystallogr Sect D Biol Crystallogr 2010;66:486–501.